The robust Fe divalent state in one unit cell FeSe/SrTiO₃ thin film

Jingdong Shen,¹ Wenxiang Jiang,² Fengfeng Zhu,³ Guan-yong Wang,⁴ Huayao Li,¹ Gan Zhao,¹ Qian Li,⁵ Wensheng Yan,⁵ Wanli Yang,⁶ Yi-De Chuang,⁶ Jin-feng Jia,^{7,8} Dong Qian,^{7,8} L. Andrew Wray,⁹, and Lin Miao¹, f

¹School of Physics, Southeast University, Nanjing 211189, China
²School of Physics and Astronomy, Shanghai Jiao Tong University, Shanghai 200240, China
³State Key Laboratory of Functional Materials for Informatics,
Shanghai Institute of Microsystem and Information Technology,
Chinese Academy of Sciences, Shanghai 200050, China
⁴Shenzhen Institute for Quantum Science and Engineering,
Southern University of Science and Technology, Shenzhen 518055, China
⁵National Synchrotron Radiation Laboratory, University of Science and Technology of China, Hefei, 230029, China
⁶Advanced Light Source, Lawrence Berkeley National Laboratory, Berkeley, California 94720, USA
⁷Key Laboratory of Artificial Structures and Quantum Control (Ministry of Education),
Shenyang National Laboratory for Materials Science, School of Physics and Astronomy,
Shanghai Jiao Tong University, Shanghai 200240, China
⁸Tsung-Dao Lee Institute, Shanghai Jiao Tong University, Shanghai 200240, China
⁹Department of Physics, New York University, New York, New York 10003, USA
(Dated: November 8, 2022)

The orbital occupancy, as the origin of Hund's rule coupling, provides critical information in understanding the multi-orbital iron-based superconductors. The one unit cell (1UC) FeSe thin film on $\rm SrTiO_3$ substrate with superconductive $T_{\rm c}$ above 60 K, has been reported with unique electronic structures as well as orbital occupancy. Here in this paper, we present the X-ray absorption spectroscopy (XAS) and resonant inelastic X-ray scattering (RIXS) study on the FeSe/STO thin films of different thicknesses. Together with the atomic multiplet simulation analysis, the FeSe/STO thin films (from 1UC to 10UC) are shown with the pure 3d6 electronic configuration which is identical to the bulk FeSe. Moreover, 1UC FeSe/STO is found to be distinctively more persistent in hosting the 3d6 configuration other than the thicker films under the oxidization process. The robustness of the 3d6 in 1UC FeSe/STO is discussed as a result of charge transfer from the substrate, as well as a mechanism to maintain the high $T_{\rm c}$ superconductivity. At last, our research calls for a further high-resolution RIXS study on the pristine superconductive 1UC FeSe/STO thin film.

I. INTRODUCTION

The epitaxial one unit cell iron selenide on the SrTiO₃ (1UC FeSe/STO), receives broad interest due to its record-breaking high superconductivity transition temperature ($T_{\rm c}\sim 65{\rm K},$ or even to 100K) within the ironbased superconductors 1-4. The T_c of 1UC FeSe/STO is about 8 times higher than its bulk crystal, raising the question about its differences with the bulk, and the core physical mechanism to enhance the superconductivity in the 1UC FeSe/STO 5. Numerous experimental efforts have been made to unveil the mystery of superconductivity enhancement in the FeSe/STO interface. The surface spectroscopic methods (STM, ARPES, etc.,) have found the resonant phonon mode, associated with the charge transfer from the TiO₂-terminated STO might play the most critical roles 6-12. These works incline to conclude that Cooper pairs in the 1UC FeSe/STO should be glued by phonons, similar to the conventional BCStype superconductors. However, there is also theoretical and experimental evidence showing that 1UC FeSe/STO is possible with magnetic ground states, in the vicinity of the antiferromagnetic quantum criticality 13-17. Such characteristics resemble the d-wave SC in cuprates. There is still an ongoing debate on the physical origin of the enhanced SC in the 1UC FeSe/STO. The detection of magnetic many-body excitation or the resonant phonon excitation would be the smoking-gun evidence to solve the puzzle. While, the thin film is believed not capable of either neutron or X-ray scattering technique. Until last year (2021), it was reported that RIXS probed the gapped non-dispersive magnetic excitation in the 1UC FeSe/STO, which is never seen in the bulk FeSe 18, 19. However, their corresponding XAS characterization shows that the '1UC FeSe' thin film under study was with a clearly different d-orbital occupancy of Fe-ion than its counterpart in bulk FeSe [20]. This discrepancy reminds that previous experimental efforts focused on the low-energy quasiparticle dynamics but Fe-valence and associated d-orbital occupancy in the 1UC FeSe is not scrutinized. The Fe outer shell in ironbased SC is nearly half-filled (3d5 or 3d6), and manifest a prominent multi-band feature [21], [22]. The Hund's rule coupling which dominates the spin alignment, is a key correlation effect within the iron-based SC [23-25]. Thus, the valence state, essential to intra-atomic exchange, provides key information in understanding the d-orbital electronic correlation effect in the iron-based high- T_c superconductivity, especially the 1UC FeSe/STO [26].

In this paper, we present the systematic study on the FeSe/STO thin films with different thicknesses (from 1UC to 100UC) by using the XAS, and the RIXS. Together with atomic multiplet simulations, we clarified that the FeSe/STO films are all with low-spin 3d6 configurations, rather than previously reported 3d5-like states. Interestingly, the Fe-ion in 1UC FeSe/STO is highly persistent with 3d6 configuration against oxidation, but thicker FeSe films trend to 3d5 outer shell under the same oxidation process. Such behavior reaffirms the massive charge transfer effect on the interface between STO and 1UC FeSe is vital to the superconductivity. Our work proves that pristine 1UC FeSe thin film of 3d6 state is a prerequisite for high-resolution RIXS experiments to detect the fundamental many-body excitations in this high $T_{\rm c}$ superconductor.

II. METHODS

All the FeSe/STO thin films are prepared by the epitaxial method (MBE), and amorphous selenium is capped to protect them against oxidation. The details of sample preparation are described in the Appendix A. All the FeSe/STO samples are transferred from the MBE chamber to the synchrotron endstation. Some of the samples immediately transferred to the experimental vacuum chamber for XAS experiment are defined as 'pristine', and other samples exposed to air for various days are defined as 'aged'. The se-capping layer is removed by annealing the sample up to 180°C inside the X-ray spectroscopy experiment chamber. Please note that the Se-capping layer of all samples was not removed until the XAS/RIXS measurement. Other details of XAS/RIXS experiments can be found in Appendix B. The probing depth of total electron yield (TEY) mode in XAS is well below ~3nm for the sub-KeV soft X-ray photons. Accordingly, the TEY signals are mostly generated from the outmost 1-2 unit cell of FeSe film for the L-edge XAS $(hv\sim710\text{eV})$ and the outmost 1 unit cell for the M-edge XAS $(hv \sim 55 \text{eV})$ 27, 28.

III. RESULTS AND DISCUSSION

First of all, to answer the question of whether the Feion in 1UC FeSe has a different valence state or orbital occupancy than the bulk FeSe or not, the Fe L-edge (2p-3d) XAS are measured. Regardless of the thicknesses, one can see the freshly prepared FeSe samples of 1UC, 2UC, and 10UC thicknesses share the same Fe L-edge XAS (fig. 1a). These XAS curves are identical to the FeSe bulk, and very similar to the Fe-metal [20] because both FeSe and Fe-metal are with metallic ground states. The long-time air-exposed FeSe thin films clearly show a different XAS spectrum, even though they are protected with amorphous selenium during the exposure. The XAS of 170 days-aged 10UC FeSe bear splitting features in

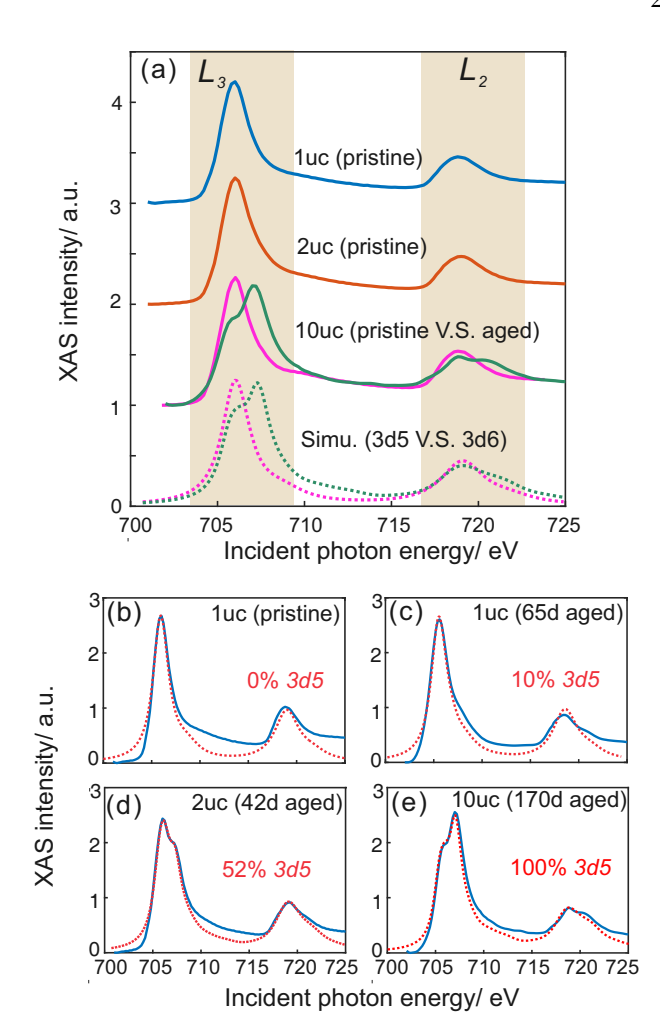


FIG. 1. The *L*-edge XAS measurement of FeSe thin films and the corresponding fittings. (a) The comparison of *L*-edge XAS curves of pristine 1UC (blue), 2UC (red) FeSe thin films, pristine (pink) and fully aged (green) 10UC FeSe thin films. The atomic multiplet simulated XAS curves of pure 3d5 (Fe³⁺, pink dashed) and 3d6 (Fe²⁺, green dashed) are present as reference. (b-e) The XAS curves (blue) of (b) pristine 1UC FeSe, (c) 65days aged 1UC FeSe, (d) 42days aged 2UC FeSe and (e) 170days aged 10UC FeSe fitted by the superpositions of simulated curves of 3d5 simulations and 3d6 simulations (red dashed). The ratio of 3d5 simulated curves of fitting results is labeled.

both L_3 and L_2 peaks, and shifted the intensity of L_3 and L_2 peaks toward higher excitation energy. Those features of the split L_3 peak resemble the XAS of 1UC FeSe in Ref [18]. The split satellite peak on the L_3 edge with higher energy observed in Ref [18] was attributed to a hybridized orbital state from the STO substrate. However, it is missing in our experiment on the pristine FeSe thin films, but similar peaks with various intensities can be found in all the aged samples under air exposure. It is well-known that the amorphous Se film relaxes and degrades over time, so it is never perfect protection for a long time of exposure to air [29] [30]. The XAS of

the aged FeSe thin films are reminiscent of the XAS of trivalent iron in the Fe_2O_3 (see fig. S4 and ref. [20]), as a natural and stable endpoint for iron oxidization in the atmosphere indicating possible oxidization in the aged FeSe thin film.

To extract the information of possible valence variation, we performed atomic multiplet simulations for the XAS spectra. The simulation details can be found in the Atomic multiplet simulations section. The divalent Feion is with a 3d6 outer shell, and the trivalent Fe-ion is with a 3d5 outer shell. Our simulation perfectly reproduces the pristine FeSe thin films by 3d6 configurations (fig. 1b), and 170 days-aged 10UC FeSe by the 3d5 configurations (fig. 1e). The 170 days aged 10UC FeSe has very similar spectra to the O₂-annealed FeSe or Fe₂O₃ 20, suggesting that the 170 days are long enough to oxidize the at least outmost unit cell of FeSe thin film to the trivalent state. Thus, the 3d5 and 3d6 simulation results are further used to estimate the oxidation level of air-exposed samples. All the samples measured by the Fe L-edge XAS were fitted by the superposition of 3d5 and 3d6 simulated curves and their oxidization level (namely, the ratio of 3d5) was extracted. For example, fig. 1d shows the fitting of XAS from 42 days-aged 2UC FeSe thin film. The XAS curve can be reproduced by the superposition of 48% ratio of the 3d6 simulation curve and 52% ratio of the 3d5 simulation curve, indicating the 2UC FeSe surface is approximately half-oxidized in

The Fe M-edge XAS (3p-3d transition) is as well employed to investigate the valence state of FeSe thin films of the different aged time. The Fe M-edge XAS curves of 1UC (10 days-aged), 2UC (30 days-aged), and 100UC (52 days-aged) FeSe thin films are significantly different (fig. 2a). One can also see that the M-edge peaks of 3d-metal are energetically narrower than the L-edge features. The M_4 and M_5 edges are located too close in the energy scale. Moreover, because of the metallic ground state of FeSe, the peaks of Fe M-edge XAS are profoundly broadened. Consequently, the M-edge XAS features are very difficult to be distinguished, and hard to extract the information by fitting directly with the 3d5 and 3d6 simulated curves. To estimate the valence state by extracting the peaks in M-edge XAS curves and fitting them with our simulated data, the negative second derivative method (SDI) is applied to all the experimental and simulation curves to exclude the background and highlight the peaks. We would also focus on the energy range from 53ev to 58ev (gray shaded in fig. 2(b-e)), where the main peaks of Fe M-edge XAS locate $\boxed{31}$. The 10 days-aged 1UC FeSe is much closer to pure 3d6 simulations but mismatches the 3d5 simulations (fig. 2b,c) indicating a nearly 100% divalence state. Fig. 2d and 2e also present the fitting results of aged 2UC FeSe and 100UC FeSe, suggesting approximately 45% and 60% trivalent Fe ion inside the two films. The details of other fitting results,

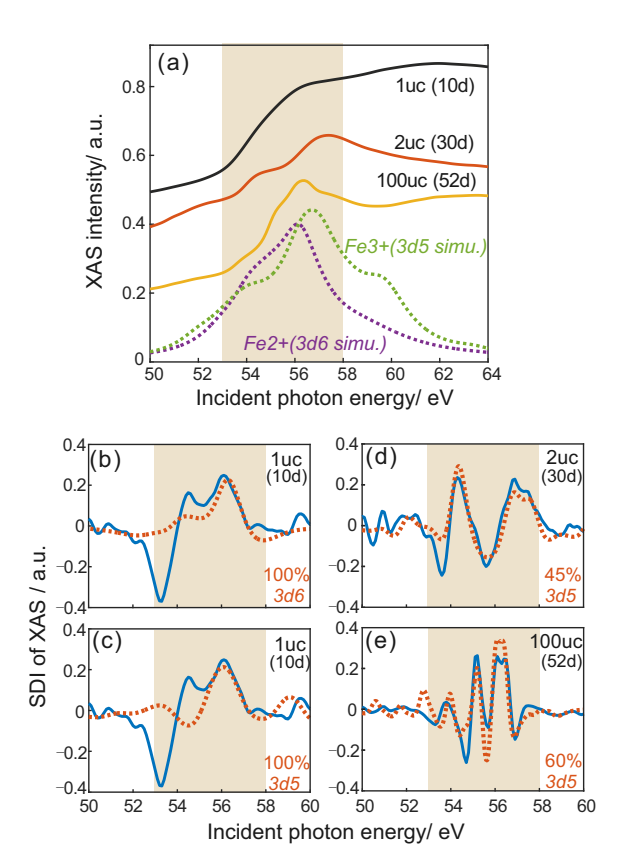


FIG. 2. The M-edge XAS measurement of FeSe thin films and the corresponding fittings. (a) The comparison of M-edge XAS curves of 10 days aged 1UC (black), 30 days aged 2UC (red), and 52 days aged 100UC (yellow) FeSe thin films. The simulated curves of pure 3d5 (Fe³⁺, cyan dashed) and 3d6 (Fe²⁺, purple dashed) are present as reference. (b-c) The 10 days aged 1UC FeSe fitted by the simulated curves from (b) 100% 3d6 configuration and (c) 100% 3d5 configuration. (d-e) The XAS curves (blue) (d) 30 days aged 2UC FeSe and (e) 52 days aged 100UC FeSe were fitted by the superpositions of simulated curves of 3d5 and 3d6 (red dashed). The ratio of 3d5 simulated curves of fitting results is labeled. The energy range from 53ev to 58ev where the Fe M-edge locates are shaded with gray color 31.

for example the aged 5UC FeSe and 10UC FeSe thin films can be found in figure S2.

When the extracted 3d5 ratio of FeSe thin films is plotted as a function of their air-exposed time, one can see that the time-dependent evolution from 3d6 to 3d5 in 1UC FeSe very much deviates from other thicknesses (Fig. 3a). For instance, under 65 days' air exposure, the 1UC FeSe thin film is with about 15% ratio of 3d5 states, while 100UC FeSe thin film gets about 60% ratio of 3d5 states after 52 days' air exposure. Due to that, all FeSe thin films are capped with the Se of identical thickness, and they should bear the same oxidization process on their surfaces. Intriguingly, Fe-ion in the 1UC FeSe thin film is more robust than other thicknesses to retain the 3d6 outer shell under air exposure. An ex-

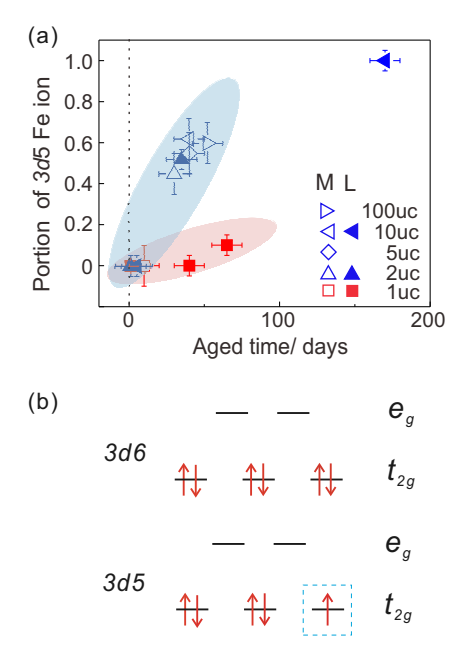


FIG. 3. The valence evolution as a function of air-exposure time. (a) The 3d5 portion extracted from the fitting of the pristine/aged FeSe thin films of different thicknesses. The data extracted from the M-edge XAS curves are marked with empty shapes and the L-edge XAS data are marked with filled shapes. The data of 1UC FeSe thin film is labeled in red color. The detailed XAS information included in this figure, as well as their fittings, are present in figure 1, figure 2, supplementary figure S2, and figure S3. (b) The low-spin 3d5 and 3d6 outer shell occupancy under the crystal field splitting of positive $10\mathrm{Dq}$.

plicit explanation is that Fe-ion in 1UC FeSe thin films are oxidized to trivalent, meanwhile, they receive extra electrons to compensate for the loss of charges. In other words, there must be a charge source to revert the oxidized Fe-ions from the 3d5 configuration to the 3d6configuration simultaneously. This charge source very much plays a role that is similar to the Lithium or the Natrium in the LiFeAs/NaFeAs, in which Fe-ion should be trivalent within the FeAs layer but manifest the divalency from XAS [32]. This mechanism can be directly associated with the profound charge transfer effect in the FeSe/STO interface. The doping of charges is found an essential avenue to give rise to an N-type Fermi surface. The STM, ARPES, and TEM work affirmed that such charge transfer effect is confined within the interfacial single UC FeSe, which explains why only 1UC FeSe thin film is more robust to keep the 3d6 valence state.

Previous ARPES measurements and DFT calculations suggest that the electron-doping from the substrate is about 0.1 to 0.15 electrons per Fe-ion when it is of the 3d6 valence state $\boxed{10}$, $\boxed{33}$, which is only about 20%-30% of charge transfer value (0.5 electrons per Fe-ion) extract from in Fig. 3a. One reason for this difference is that the 3d5 valence state has a lower chemical potential than the

3d6 valence state, resulting in extra potential difference and thus more electron doping from the substrate. The other reason that atomic multiplet simulation is based on the molecular orbital theory, is by assuming the materials are insulators. The itinerancy of the 3d6 valence state in FeSe is omitted by the simulation, which magnifies the fitting errors. Accordingly, it is noteworthy that the deviation of the 3d5 ratio extracted from the atomic multiplet simulation could be smaller than the real situation.

Whether a 3d5 or 3d6 outer shell will give rise to significantly different electronic and magnetic ground states. By consideration of the octahedral crystal field where the t_{2g} orbital is lower in energy, the 3d6 would occupy all the t_{2g} orbitals but the 3d5 will leave one electron unpaired (Fig. 3b). Although the crystal field of FeSe is in fact between an octahedral scenario and a tetrahedral scenario, and the e_g and t_{2g} orbital are possibly intertwined [22], the 3d5 outer shell configuration would be more susceptible to the magnetic order. Moreover, a recent PES work suggests 3d5 outer shell would also appear in the non-superconductive FeSe thin film when it is not sufficiently annealed after the sample growth [34], which also sets up the correspondence between the 3d6 valence state and the superconductivity in 1UC FeSe/STO.

Due to the reason no appropriate experimental method to probe the many-body excitation in ultra-thin films, it has been a long debate about whether magnetic excitation exists in the parent phase of the FeSe thin film. RIXS is proven to be a high-efficiency scattering method to reveal the magnon in the single crystal of cuprates and iron-based superconductivity. RXIS study on the FeSe thin films was first reported in Ref. [18] and found it capable of detecting the possible magnetic excitation. Our discussion above indicates that the 1UC FeSe sample under study was possibly partially oxidized, and the excitations could be a result of the 3d5 valence state, which is more susceptible to magnetism.

As well, we have performed the RIXS measurements on the pristine 10UC FeSe thin film (Fig. 4a-b) and the fully oxidized 10UC FeSe (Fig. 4c-d). Due to the limited energy resolution (~500meV) of our apparatus, the RIXS excitation peaks are very broad and we are not aimed at discovering fine peaks (Fig. 4b,d). The most pronounced discrepancy between the two sets of RIXS data is the elastic scattering signal (energy loss=0 eV). On the pristine 10UC FeSe, a candidate peak of elastic scattering arises only at the incident photon energy of 708 eV but is missing when the incident photon energy locates at the peak of Fe L_3 -edge. For the oxidized 10UC FeSe, one can see that the elastic scattering peak is overwhelmingly high when the incident energy is tuned to Fe L_3 -edge. Such an intensive elastic peak of Fe L-edge RIXS is not usually seen in other divalent iron-based superconductors [35, 36], but can be observed in the trivalent Fe (e.g., Fe_2O_3) 37 and the previously

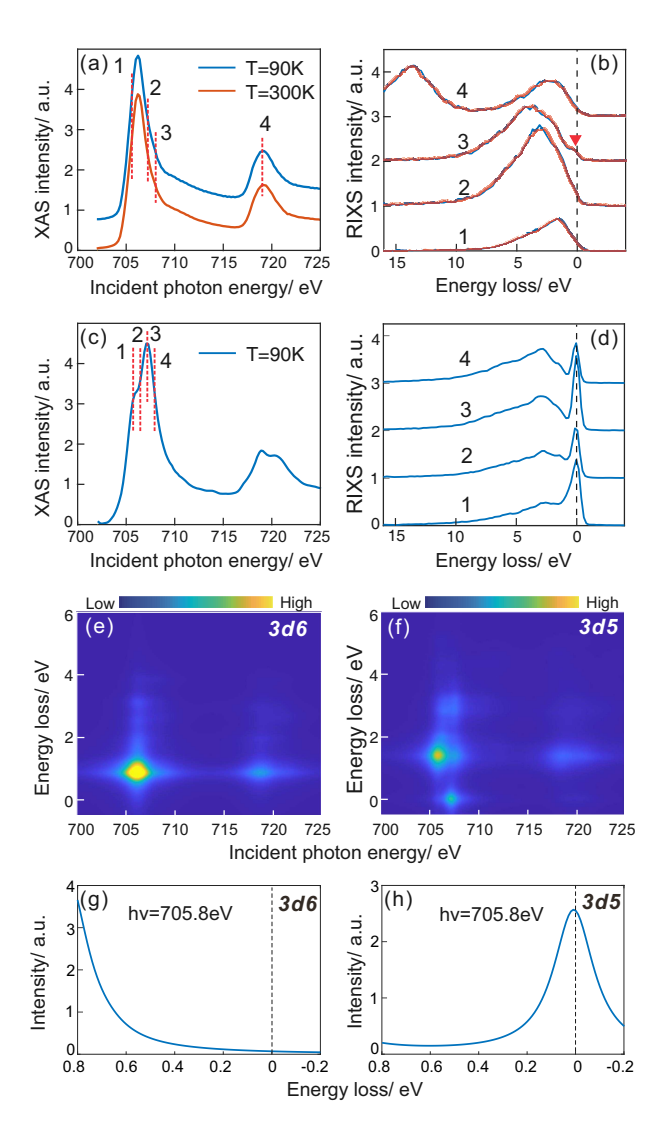


FIG. 4. The RIXS measurement and corresponding RIXS simulations of the 10UC FeSe thin film. (a) The L-edge XAS of pristine 10UC FeSe at T=90K (blue) and 300K (red). The incident photon energy for following RIXS measurement is marked by the vertical dashed lines. (b) The RIXS curves of four different incident photon energies ($hv = 705.6 \,\text{eV}$, $707.2 \,\text{eV}$, $708 \,\text{eV}$ and $719 \,\text{eV}$) at T=90K (blue) and T=300K (red). (c) The L-edge XAS of 170 days aged 10UC FeSe at T=90K. The incident photon energy for following RIXS measurement is marked by the vertical dashed lines. (d) The RIXS curves of four different incident photon energies (hv=705.8eV, 706.4eV, 707eV and 707.6eV) at T=90K. (e-f) The simulated RIXS map with (e) 3d6 outer shell and (f) 3d5 outer shell. (g-h) The simulated RIXS curves with (g) 3d6 outer shell and (h) 3d5 outer shell with incident photon energy of hv=705.8eV.

reported RIXS of FeSe/STO (Fig. S14 in Ref $\boxed{18}$). To further justify our analysis of experiments, we performed the RIXS simulations. When the incident photon energy is tuned to L_3 -edge, the simulated RIXS of the 3d6 basis shows almost negligible elastic scattering signals (Fig. 4e,g), but the simulated RIXS of 3d5 will give rise to a

considerable elastic peak (Fig. 4f,h). Accordingly, our RIXS experiments and simulations show high consistency that the elastic peak could be a good index to monitor the oxidization of FeSe thin films. That means the elastic peak could appear in the Fe *L*-edge RIXS with relative small intensity, and one needs to be very cautious if its intensity is overwhelmingly high.

IV. CONCLUSIONS

To conclude, our XAS&RIXS study on FeSe/STO thin films unambiguously reveals that FeSe thin films have the same 3d6 outer shell of Fe-ion as the bulk FeSe. Meanwhile, the 1UC FeSe is surprisingly robust to host the 3d6 valence state, and the charge transfer from the substrate is potentially the reason. We discussed that the charge transfer effect is uniquely essential because the 3d6 orbital occupancy in 1UC FeSe is key to preserving its superconductivity. The previous study suggests that 1UC FeSe thin film is suitable for RIXS study to explore the possible magnetic excitations, but the present work indicates that the pristine FeSe thin film of divalence is necessary for probing the possible many-body excitations, as signatures for the electronic correlation.

ACKNOWLEDGEMENTS

L.M. was supported by the National Natural Science Foundation of China (Grants No. U2032156 and No. 12004071), Ministry of Science and Technology of China (Grants No. 2022YFA1405700), Natural Science Foundation of Jiangsu Province, China (Grant No. BK20200348), and the program of Jiangsu specially-appointed professor. This research used resources of the Advanced Light Source, a U.S. DOE Office of Science User Facility under Contract No. DE-AC02-05CH11231. L.A.W. acknowledges the support of the National Science Foundation under Grant No. DMR-2105081.

Appendix A: Materials

The FeSe thin films were epitaxially grown on the Nb-doped (0.7%) SrTiO₃ substrate, following a standard procedure [2], [17]. All the films were post-annealed at ~ 500 °C for 1 hour after growth. The crystalline quality of FeSe thin films were monitored by the RHEED (see Fig. S1). The STM/STS is used to confirm the atomic-flat surface morphology and the superconductivity in the 1UC FeSe/STO (see Fig. S1). All the FeSe thin films are capped with amorphous selenium with a thickness of tens of nanometers before taking them out from the MBE chamber.

Appendix B: Experimental method

The soft X-ray absorption (Fe L-edge) spectroscopy and the related RIXS were performed in the iRIXS end-station at beamline 8 of Advanced Light Source and the Beamlines MCD-A and MCD-B (Soochow Beamline for Energy Materials) at NSRL. The integrated resolution of the RIXS is about 1000, which is about \sim 700 meV at hv=700 eV. The RIXS measurements were with a fixed incidence angle of 30° and an exit angle of 60°. The UV X-ray absorption (Fe M-edge) spectroscopy was performed in the MERIXS endstation at BL4.0.1 of Advanced Light Source. The XAS was taken at temperature T=90K (Fe L-edge) and 10K (Fe M-edge) if no specific notes.

Appendix C: Atomic multiplet simulations

Atomic multiplet calculations were performed as in ref. 38 and 39, describing $2p^6$ $3d^n \rightarrow 2p^5$ $3d^{n+1}$ (*L*-edge) or $3p^6$ $3d^n \rightarrow 3p^5$ $3d^{n+1}$ (M-edge) X-ray absorption in the dipole approximation. Hartree-Fock parameters were obtained from the Cowan code 40, and full diagonalization of the multiplet Hamiltonian was performed using LAPACK drivers [41]. The crystal field splitting energy (10Dq) was set to 0.9 eV for the 3d6 ground state. We have noticed that the 10Dq value was extracted as ~0.5 eV in from the study on (Li,Fe)OHFeSe compound 42. An extensive comparison (see supplementary fig. S5) show that the simulated XAS lineshapes are highly similar with $10\mathrm{Dq}$ values varied from $0.4~\mathrm{eV}$ to $1~\mathrm{eV}$. Meanwhile, the 10Dq value was set to 1.5 eV for 3d5ground state, which maybe due to the formation of Fe₂O₃ 43.

The atomic multiplet simulation parameters used in the M-edge are nearly identical to the L-edge, except the interaction coefficient (F $_{g~p-d}$) between the 2p-3d orbital (L-edge) is renormalized to 66% of the 3p-3d orbital (M-edge).By fitting the M-edge XAS of FeSe and its oxidate, the relative energy shift between the 3d6 simulated XAS curves and 3d5 simulated XAS curves is a function of FeSe thickness. The relative shift energy is 0.6 eV (1UC FeSe), 3 eV (2UC, 5UC, and 10UC FeSe) and -0.4 eV (100UC).

- * Electronic address: dqian@sjtu.edu.cn; Corresponding author
- † Electronic address: lawray@nyu.edu Corresponding author
- ‡ Electronic address: lmiao@seu.edu.cn; Corresponding author

- [1] Q.-Y. Wang, Z. Li, W.-H. Zhang, Z.-C. Zhang, J.-S. Zhang, W. Li, H. Ding, Y.-B. Ou, P. Deng, K. Chang, et al., Chin. Phys. Lett. 29, 037402 (2012).
- [2] W.-H. Zhang, Y. Sun, J.-S. Zhang, F.-S. Li, M.-H. Guo, Y.-F. Zhao, H.-M. Zhang, J.-P. Peng, Y. Xing, H.-C. Wang, et al., Chin. Phys. Lett. 31, 017401 (2014).
- [3] J.-F. Ge, Z.-L. Liu, C. Liu, C.-L. Gao, D. Qian, Q.-K. Xue, Y. Liu, and J.-F. Jia, Nature Commun. 14, 285 (2015).
- [4] Z. Zhang, Y.-H. Wang, Q. Song, C. Liu, R. Peng, K. Moler, D. Feng, and Y. Wang, Sci. Bull. 60, 1301 (2015).
- [5] F.-C. Hsu, J.-Y. Luo, K.-W. Yeh, T.-K. Chen, T.-W. Huang, P. M. Wu, Y.-C. Lee, Y.-L. Huang, Y.-Y. Chu, D.-C. Yan, et al., P. Natl. Acad. Sci. USA 105, 14262 (2008).
- [6] J. Lee, F. Schmitt, R. Moore, S. Johnston, Y.-T. Cui, W. Li, M. Yi, Z. Liu, M. Hashimoto, Y. Zhang, et al., Nature 515, 245 (2014).
- [7] Y. C. Tian, W. H. Zhang, F. S. Li, Y. L. Wu, Q. Wu, F. Sun, G. Y. Zhou, L. Wang, X. Ma, Q.-K. Xue, and J. Zhao, Phys. Rev. Lett. 116, 107001 (2016).
- [8] C. Tang, C. Liu, G. Zhou, F. Li, H. Ding, Z. Li, D. Zhang, Z. Li, C. Song, S. Ji, K. He, L. Wang, X. Ma, and Q.-K. Xue, Phys. Rev. B 93, 020507(R) (2016).
- [9] D. Liu, W. Zhang, D. Mou, J. He, Y.-B. Ou, Q.-Y. Wang, Z. Li, L. Wang, L. Zhao, S. He, et al., Nature Commun. 3, 931 (2012).
- [10] S. He, J. He, W. Zhang, L. Zhao, D. Liu, X. Liu, D. Mou, Y.-B. Ou, Q.-Y. Wang, Z. Li, et al., Nature Mater. 12, 605 (2013).
- [11] S. Tan, Y. Zhang, M. Xia, Z. Ye, F. Chen, X. Xie, R. Peng, D. Xu, Q. Fan, H. Xu, et al., Nature Mater. 12, 634 (2013).
- [12] H. Zhang, D. Zhang, X. Lu, C. Liu, G. Zhou, X. Ma, L. Wang, P. Jiang, Q.-K. Xue, and X. Bao, Nature Commun. 8, 214 (2017).
- [13] K. Liu, Z.-Y. Lu, and T. Xiang, Phys. Rev. B 85, 235123 (2012).
- [14] C. Tresca, F. Ricci, and G. Profeta, 2D Mater. 2, 015001 (2014).
- [15] H.-Y. Cao, S. Chen, H. Xiang, and X.-G. Gong, Phys. Rev. B 91, 020504(R) (2015).
- [16] Z. Wang, H. Zhang, D. Liu, C. Liu, C. Tang, C. Song, Y. Zhong, J. Peng, F. Li, C. Nie, et al., Nature Mater. 15, 968 (2016).
- [17] Y. Zhou, L. Miao, P. Wang, F. F. Zhu, W. X. Jiang, S. W. Jiang, Y. Zhang, B. Lei, X. H. Chen, H. F. Ding, H. Zheng, W. T. Zhang, J.-f. Jia, D. Qian, and D. Wu, Phys. Rev. Lett. 120, 097001 (2018).
- [18] J. Pelliciari, S. Karakuzu, Q. Song, R. Arpaia, A. Nag, M. Rossi, J. Li, T. Yu, X. Chen, R. Peng, et al., Nature Commun. 12, 3122 (2021).
- [19] M. C. Rahn, K. Kummer, N. B. Brookes, A. A. Haghighirad, K. Gilmore, and A. T. Boothroyd, Phys. Rev. B 99, 014505 (2019).
- [20] D. Telesca, Y. Nie, J. I. Budnick, B. O. Wells, and B. Sinkovic, Phys. Rev. B 85, 214517 (2012).
- [21] H. Hu, R. Yu, E. M. Nica, J.-X. Zhu, and Q. Si, Phys. Rev. B **98**, 220503(R) (2018).
- [22] R. M. Fernandes and A. V. Chubukov, Rep. Prog. Phys. 80, 014503 (2016).
- [23] A. Kostin, P. O. Sprau, A. Kreisel, Y. X. Chong, A. E. Böhmer, P. C. Canfield, P. J. Hirschfeld, B. M. Andersen, and J. Davis, Nature Mater. 17, 869 (2018).

- [24] Z. Yin, K. Haule, and G. Kotliar, Nature Mater. 10, 932 (2011).
- [25] S. Mandal, P. Zhang, S. Ismail-Beigi, and K. Haule, Phys. Rev. Lett. 119, 067004 (2017).
- [26] A. Georges, L. d. Medici, and J. Mravlje, Annu. Rev. Condens. Matter Phys. 4, 137 (2013).
- [27] M. Abbate, J. Goedkoop, F. De Groot, M. Grioni, J. Fuggle, S. Hofmann, H. Petersen, and M. Sacchi, Surf Interface Anal 18, 65 (1992).
- [28] S. Schroeder, G. Moggridge, R. Ormerod, T. Rayment, and R. Lambert, Surf sci 324, L371 (1995).
- [29] W. C. Tan, G. Belev, K. Koughia, R. Johanson, S. K. O'Leary, and S. Kasap, J. Mater. Sci. Mater. Electron. 18, 429 (2007).
- [30] H. Lin, C. Cheng, K. Chen, C. Tseng, S. Huang, M. Chang, S. Tseng, M. Hong, and J. Kwo, APL Mater. 6, 066108 (2018).
- [31] J. Vura-Weis, C.-M. Jiang, C. Liu, H. Gao, J. M. Lucas, F. M. De Groot, P. Yang, A. P. Alivisatos, and S. R. Leone, J. Phys. Chem. Lett. 4, 3667 (2013).
- [32] E. Kurmaev, J. McLeod, N. Skorikov, L. Finkelstein, A. Moewes, Y. A. Izyumov, and S. Clarke, J. Phys.: Condens. Matter 21, 345701 (2009).
- [33] Y. Zhou and A. J. Millis, Phys. Rev. B 93, 224506 (2016).
- [34] H. Wang, A. Ghosh, C. Wang, S. Hsieh, Y. Shao, J. Chiou, C. Chen, C. Pao, J. Lee, Y. Liu, et al., P. Natl. Acad. Sci. USA 116, 22458 (2019).
- [35] W. L. Yang, A. P. Sorini, C.-C. Chen, B. Moritz, W.-S. Lee, F. Vernay, P. Olalde-Velasco, J. D. Denlinger, B. Delley, J.-H. Chu, J. G. Analytis, I. R. Fisher, Z. A.

- Ren, J. Yang, W. Lu, Z. X. Zhao, J. van den Brink, Z. Hussain, Z.-X. Shen, and T. P. Devereaux, Phys. Rev. B 80, 014508 (2009).
- [36] X. Lu, W. Zhang, Y. Tseng, R. Liu, Z. Tao, E. Paris, P. Liu, T. Chen, V. N. Strocov, Y. Song, R. Yu, Q. Si, P. Dai, and T. Schmitt, Nature Physics 18, 806 (2022).
- [37] J. Miyawaki, S. Suga, H. Fujiwara, M. Urasaki, H. Ikeno, H. Niwa, H. Kiuchi, and Y. Harada, Phys. Rev. B 96, 214420 (2017).
- [38] L. A. Wray, J. Denlinger, S.-W. Huang, H. He, N. P. Butch, M. B. Maple, Z. Hussain, and Y.-D. Chuang, Phys. Rev. Lett. 114, 236401 (2015).
- [39] L. Miao, R. Basak, S. Ran, Y. Xu, E. Kotta, H. He, J. D. Denlinger, Y.-D. Chuang, Y. Zhao, Z. Xu, et al., Nature Commun. 10, 644 (2019).
- [40] R. D. Cowan, "Robert d. cowan's atomic structure code," (1996), https://www.tcd.ie/Physics/people/Cormac. McGuinness/Cowan/.
- [41] E. Anderson, Z. Bai, C. Bischof, L. S. Blackford, J. Demmel, J. Dongarra, J. Du Croz, A. Greenbaum, S. Hammarling, A. McKenney, et al., LAPACK Users' guide (SIAM, 1999).
- [42] Q. Xiao, W. Zhang, T. C. Asmara, D. Li, Q. Li, S. Zhang, Y. Tseng, X. Dong, Y. Wang, C.-C. Chen, et al., arXiv preprint arXiv:2110.05361 (2021).
- [43] N. Zhang, C. Liu, J.-L. Zhao, T. Lei, J.-O. Wang, H.-J. Qian, R. Wu, L. Yan, H.-Z. Guo, and K. Ibrahim, Chinese Physics B 25, 097402 (2016).